metals

MDPI

Article

Effects of Different Fouling Organisms on Corrosion Behavior of Carbon Steel in Dalian Seawater

Wanbin Chen, Yihan Wang, Mingyu Wang, Yi Huang and Yunze Xu *

School of Naval Architecture and Ocean Engineering, Dalian University of Technology, Dalian 116024, China; cwb173@mail.dlut.edu.cn (W.C.); yh_w1998@mail.dlut.edu.cn (Y.W.); mingyu.w@foxmail.com (M.W.); huangyi@dlut.edu.cn (Y.H.)

* Correspondence: xuyunze@dlut.edu.cn

Abstract: Carbon steels are widely used in ocean engineering due to their cost effectiveness, ease of manufacture, and excellent weldability. However, the attachment of macro-fouling organisms in seawater poses a serious threat to the integrity of carbon steel structures. In this experiment, carbon steel plates were immersed in the Dalian Sea area from January to October to investigate the effects of macro-fouling on corrosion propagation. The electrochemical measurement indicated that the propensity for the corrosion of Q235B is ranked as ascidians > mussels > barnacles. The characterization results indicated that various marine organisms significantly influenced the corrosion behavior of Q235B carbon steel immersed in natural seawater. The colonization of barnacles inhibited corrosion at the barnacle central area, and the presence of barnacle covering caused crevice corrosion at the edges of the barnacle due to oxygen concentration cells. The presence of ascidians resulted in general corrosion due to the locally high conductivity and ion diffusion rate. A relatively compact rust layer, which exhibited localized defects, was observed beneath the mussels. Seawater had the ability to penetrate the rust layer through these defects, leading to the formation of pitting corrosion on the metal substrate.

Keywords: fouling organisms; Dalian Sea area; carbon steel; rust layer; localized corrosion

check for updates

Citation: Chen, W.; Wang, Y.; Wang, M.; Huang, Y.; Xu, Y. Effects of Different Fouling Organisms on Corrosion Behavior of Carbon Steel in Dalian Seawater. *Metals* **2023**, *13*, 1503. https://doi.org/10.3390/met13091503

Academic Editor: Branimir N. Grgur

Received: 2 August 2023
Revised: 19 August 2023
Accepted: 20 August 2023
Published: 22 August 2023

Copyright: © 2023 by the authors. Licensee MDPI, Basel, Switzerland. This article is an open access article distributed under the terms and conditions of the Creative Commons Attribution (CC BY) license (https://creativecommons.org/licenses/by/4.0/).

1. Introduction

Carbon steels are extensively utilized in ocean engineering due to their low cost, manufacturability, weldability, etc. [1,2]. However, carbon steel is susceptible to significant corrosion risks when exposed to seawater due to its low corrosion resistance [3]. Moreover, corrosion damage to carbon steel might be more severe and localized due to the covering of marine macro-fouling organisms on the surface of the steel [4]. The adhesion of macro-fouling organisms could change steel surface properties, resulting in the formation of oxygen concentration cells between the organism-covered area and the non-covered area [5]. Secretions of macro-fouling organisms could cause local acidification and the enrichment of chloride ions on a steel substrate, accelerating localized corrosion [6].

Different marine areas might be inhabited by different macro-fouling organisms. The differences between main macro-fouling organisms might cause significant variations in the corrosion patterns. Blackwood studied the localized corrosion of stainless steel caused by macro-fouling organisms in the Singapore Sea area [7]. Their results showed that oysters caused extensive localized corrosion of 316L stainless steel. Only slight crevice corrosion was found beneath dead barnacles, while no corrosion was observed beneath green mussels. However, Zhang found that barnacles caused the most serious localized corrosion of 316L stainless steel in the Xiamen Sea area [8]. Crevice corrosion initiated at the edge of the shell base and then resumed inward, proposing that more severe corrosion occurs at barnacle edges due to IR drop. Chen found that the macro-fouling organisms that adhered to 316L stainless steel in the Dalian Sea area are mainly barnacles, ascidians, and mussels [9]. Localized corrosion was observed at both the barnacle edge and center. The perforation

of the steel mostly occurred in the central area, which is different from that in the Xiamen Sea area, while the covering of ascidians could mitigate the localized corrosion induced by barnacles. Wang et al. studied the corrosion of AISI 4135 carbon steel covered by the main macro-fouling organisms in the port of Jiaozhou Bay in the Yellow Sea in China [5,6]. The main macro-fouling organisms were barnacles in the middle tide region. The main macro-fouling organisms were oysters and ascidians in the low tide region. Two types of oyster fouling were found on the steel in this sea area. The oysters were tightly attached to the steel surface in some areas, which inhibits the corrosion process due to the isolation of the steel substrate from seawater. However, oyster/steel gaps were found on the steel surface, which facilitates the formation of oxygen concentration cells, causing crevice corrosion. The corrosion performance of AISI 4135 steel covered by barnacles was similar to that of oysters. Ascidians could cause a uniform corrosion pattern due to their high conductivity and ion diffusivity ability, which has nearly no influence on seawater exchange. Ma reported the results of an 8-year real sea test of domestic carbon steel in three marine experimental stations in the Yellow Sea, the East China Sea, and the South China Sea [10]. According to the results of fouling organism adhesion and carbon steel corrosion, biological fouling can reduce the average corrosion rate of carbon steel but promote localized corrosion in the coastal waters of the East and South China Seas where fouling organisms are active. As a result, different marine organisms growing in different sea areas may cause dramatic differences in corrosion patterns. Even in the same sea area, the attached marine organisms can also be different, resulting in different corrosion patterns.

Dalian is an important port city in China, where a new seadrome and offshore wind farms are being prepared for construction. Carbon steel will be used as the main building material. Macro-fouling corrosion is a great threat to the steel structures in the Dalian Sea area. However, the macro-fouling corrosion of carbon steel in the Dalian Sea area has rarely been studied. Seawater temperatures are low in winter in the Dalian Sea area, which is not conducive to the growth of marine organisms. However, marine organisms tend to grow quickly after March, resulting in totally different marine environments in comparison with the southern sea areas of China. Accordingly, the corrosion performance of Q235B carbon steel is studied in this work for 9 months of immersion testing in the Dalian Sea area. The corrosion patterns of carbon steel beneath different macro-fouling organisms are understood according to the test results.

2. Materials and Methods

The immersion test of the Q235B carbon steel was conducted in a bay of the Dalian Sea area, as shown in Figure 1a. The main ion contents (g L^{-1}) of the natural seawater are Cl^- 17.09, Na^+ 9.45, $SO_4{}^{2-}$ 2.20, Mg^{2+} 1.06, Ca^{2+} 0.03, K^+ 0.26, HCO^{3-} 0.13, Br^- 0.03. The pH of the natural seawater was measured at around 8.21. The immersed steel plates were machined in the size of 350 × 250 × 1 mm^3 and installed in a nylon frame. The main components of the steel plate (by weight%) were C 0.16, Si 0.30, Mn 0.45, P 0.045, S 0.03, Cr 0.30, Ni 0.30, Cu 0.25, and Fe balance. The steel plates were securely fastened within the nylon frame to prevent the loss of test samples due to the influence of seawater flow. The back surfaces of the steel plates were coated with epoxy paint to prevent corrosion initiation from the backside. Only one side of the sample could come into contact with the seawater at the beginning of the test. The steel plates were immersed about 0.5 m to 2.0 m below the low water line on the test platform to ensure full immersion. More details of the test platform were introduced in a previous study [9]. The test duration was 9 months, from January to October. The seawater temperature is around 0–5 °C from January to March. The seawater temperature increases to 10 °C in May. The seawater temperature further climbs to around 15–25 °C from June to October.

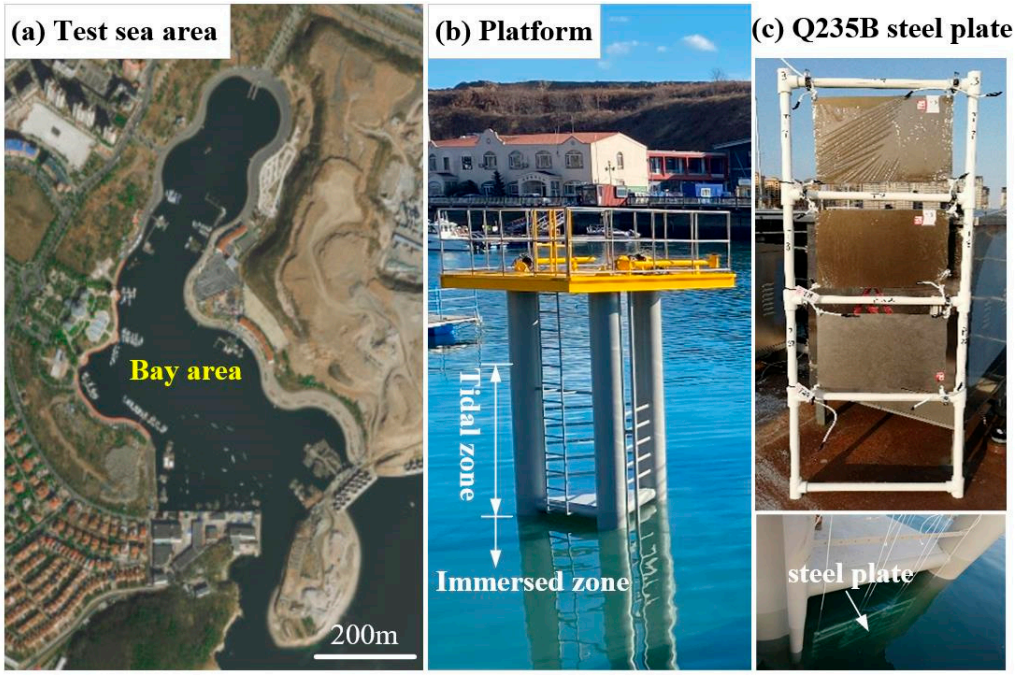


Figure 1. The local sea area for field test (**a**), the test platform (**b**), and the steel plates (**c**).

After 9 months of immersion, one of the steel plates was carefully taken out from the sea to avoid the peeling of the fouling organisms. The original macro-fouling on the steel surface after removal from the seawater was immediately photographed using an EOS digital camera (Canon, Tokyo, Japan). Thereafter, the steel surface was washed using a high-pressure water gun to eliminate the loose outer organisms. The steel surface was photographed again after washing. After general photography, some typical areas covered by different organisms were selected for electrochemical impedance spectroscopy (EIS) measurements and local morphology observation. The typical areas with different marine fouling organisms were cut into small samples (15 × 15 mm^2) from the steel plate. The remaining organisms were completely cleaned by brush washing. The EIS measurement results were tested in natural seawater after the open-circuit potential (OCP) became stable. The EIS measurement was performed using a 10 mV sinusoidal signal around OCP in the frequency range of 10^5–10^{-1} Hz. The measurement results were fitted using ZSimpWin (DEMO, Ametek Inc., Berwyn, PA, USA). Then, the formed secretory and rust layer beneath the different kinds of marine organisms from the Dalian Sea area were observed using EM-30+ scanning electron microscopy (SEM, Coxem, Daejeon, Korea) in conjunction with energy-dispersive spectroscopy (EDS) measurements. Then, cross-section views of these typical areas were also observed using SEM. The structures of the rust layers were further studied using laser confocal micro-Raman spectra (DXR3xi, Thermo Fisher^{TM}, Waltham, MA, USA). Finally, the rust layers on the small samples were cleaned using an acid agent, as suggested by ASTM G1-03. The 3D profiles of these corroded areas were measured using an OLS 5000 infinite microscope (Olympus, Tokyo, Japan) to analyze the localized corrosion performance under different macro-fouling marine organisms.

3. Results

3.1. Macro-Morphology of the Steel Plate with Different Marine Organisms

Figure 2a shows the macro-morphology of the Q235B steel plate taken out from the seawater. It was observed that the main marine fouling organisms in the Dalian Sea area consist of barnacles, ascidians, and mussels. Figure 2b shows the macro-morphology of the steel plate after washing with a water gun. It can be observed that the ascidians and mussels were totally removed from the steel surface, while most of the barnacles remained on the steel surface, indicating the strong adhesion strength of the barnacles. As shown in

Figure 2b, three typical areas could be identified from the coverings of the different marine organisms. The local areas mainly covered by barnacles were defined as Zone 1. The local areas mainly covered by ascidians were defined as Zone 2, where the rust layer presented as reddish brown and gelatinous. The local areas mainly covered by black mussels were defined as Zone 3, where a relatively compact black layer could be observed.

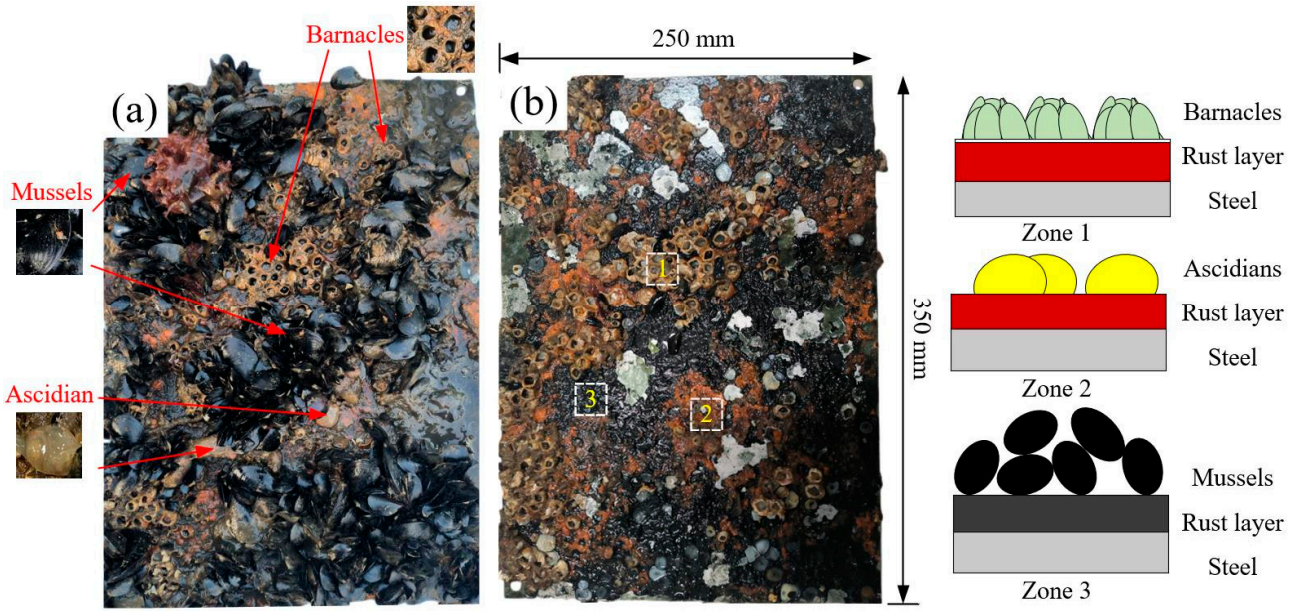


Figure 2. The photos of the whole steel plate (**a**) immediately taken out of the seawater (**b**) after the removal of the loose outer organisms.

3.2. The Interface Electrochemistry at Three Typical Areas

The EIS measurement results of Samples 1–3 (Figure 3b), which were cut from the selected zone (Figure 2b), are plotted in Figure 3a. It can be seen that Sample 1, which was selected from Zone 1, was covered by barnacles (the green color in Figure 3c). Sample 2, on which the rust layer presents as reddish brown and gelatinous, was selected from Zone 2, and Sample 3, on which the rust layer presents as a compact black layer, was selected from Zone 3. Equivalent circuits with two time constant models (Figure 3c) were employed to fit Samples 1–3 [6], where R_s is the solution resistance, R_f is the pore resistance between macrofouling/steel or rust resistance, R_{ct} is the charge transfer resistance, W is the Warburg impedance element, and Q_c and Q_{dl} are capacitance between macrofouling/steel or rust capacitance and double-layer capacitance, respectively.

The fitted parameters are listed in Table 1. $R_f + R_{ct}$ often reflects the level of rust compactness and the resistance to corrosion. A higher value for $R_f + R_{ct}$ indicates a lower corrosion rate [11]. It is evident that Sample 1 displayed the highest R_f value, which was 30 times greater than that of Samples 2 and 3. This signifies that barnacle-covered areas had lower corrosion rates compared to ascidians and mussels. The protective effect of the rust layer was improved due to the adhesion of the barnacles. This was mainly attributed to the presence of barnacle cement, which has lower electrical conductivity and hinders the diffusion of ions and oxygen [5]. Sample 2 displayed the lowest R_f value. This is due to the Cl^- enriched by the secretion of ascidians, which can destroy the compactness of the rust layer and thereby weaken its protective properties [6,12]. The resistance value of Sample 3 was between that of Sample 1 and Sample 2. Mussels normally adhere to steel through filamentous secretions [13], which has fewer effects on the rust layer. In general, the propensity for the corrosion of Q235B is ranked as ascidians > mussels > barnacles.

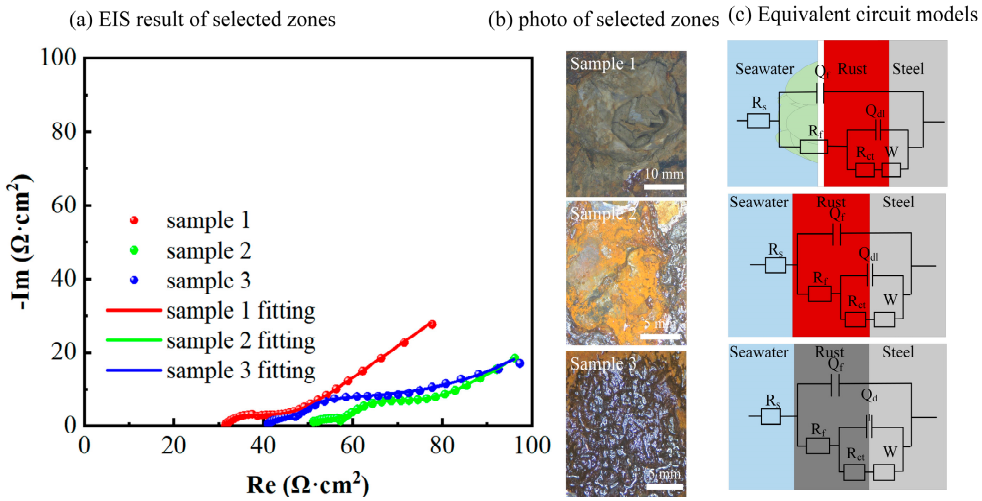


Figure 3. The EIS measurement. (**a**) The Nyquist plots of the selected areas, (**b**) the photos of the selected areas, and (**c**) the equivalent circuit used for EIS fitting.

Table 1. The fitted parameters of the EIS measurement results for different surface conditions.

Specimen	R_s ($\Omega \cdot cm^2$)	R_f ($\Omega \cdot cm^2$)	Q_f–Y_0 ($10^{-5} \times \Omega^{-1} \cdot cm^{-2} \cdot s^n$)	Q_f–n	R_{ct} ($\Omega \cdot cm^2$)	Q_r–Y_0 ($10^{-5} \times \Omega^{-1} \cdot cm^{-2} \cdot s^n$)	Q_r–n	W-Y_0 ($10^{-5} \times \Omega^{-1} \cdot cm^{-2} \cdot s^n$)
Sample 1	31.75	1000	0.51	0.99	28.65	79.44	0.80	0.0349
Sample 2	47.12	23.56	96.76	0.23	25.71	57.83	0.99	0.0605
Sample 3	38.06	32.37	100.40	0.26	46.69	9.43	0.94	0.0487

3.3. The Structure and Components of the Rust Layer for Three Typical Areas

According to the macro-morphology observations, it was found that the species of the organisms had a significant influence on the formed rust layer. In order to figure out the structure and components of the rust layer that formed beneath the different marine organisms, the micro-morphologies of the rust layer in the three typical areas were further characterized. The yellow "+" symbol is the measurement area of the EDS result.

Figure 4a shows the general micro-morphology of the rust layer with the removal of the barnacles on Zone 1 by brush washing. It can be seen that the barnacle cement closely adheres to the steel surface, the main components of which are Ca, C, and O elements. The EDS results indicate that the barnacle cement attached to the carbon steel is a calcium layer. The breakdown of the barnacle occurs when brushing away the barnacle shells. The different shapes of the corrosion products can be observed beneath the barnacle cement. The "hole"- and "plate"-like corrosion products can be seen in Figure 3b. It can further be seen from Figure 3c, with higher magnification, that the "hole"-like rust in Local Area 1 presents as doughnut-shaped. Based on the atomic ratios of Fe and O elements (0.77), it can be deduced that the doughnut-shaped rust is mainly composed of Fe_3O_4 [14]. As shown in Figure 4d, the "plate"-like corrosion products in Local Area 2 present as bird nest forms, and the ratio of Fe and O is close to 0.5, indicating that the main composition of the rust layer in Local Area 2 might be γ-FeOOH [15]. These observation results suggest that corrosion may still occur beneath the barnacle cement, resulting in the formation of Fe_3O_4 and γ-FeOOH.

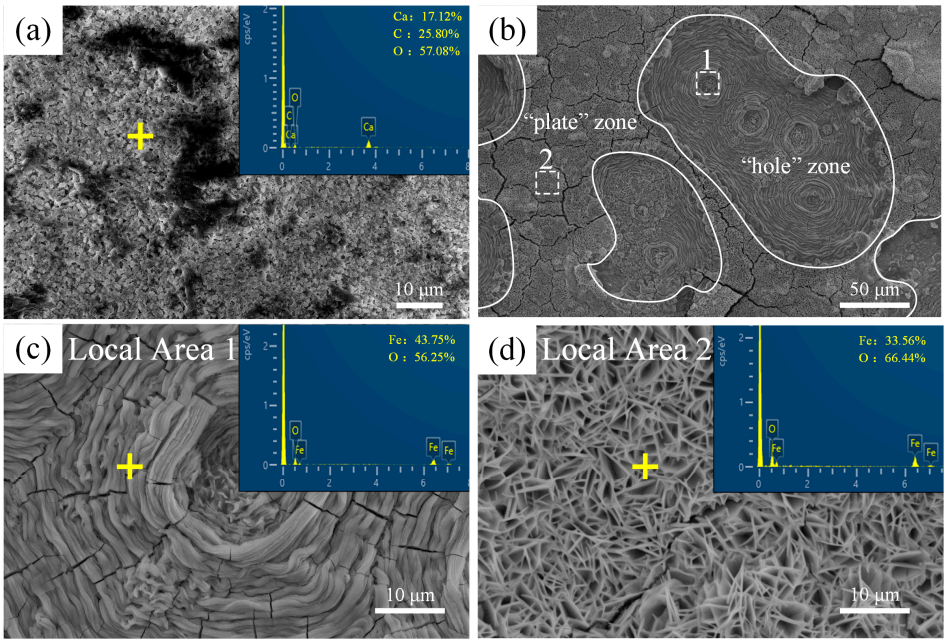


Figure 4. The micro-morphologies of the rust layers formed beneath the barnacles: (**a**) the barnacle cement and (**b**) the rust layers formed beneath the barnacle cement. The enlargement of local areas in Figure 4b: (**c**) Local Area 1 and (**d**) Local Area 2.

Figure 5a shows a general view of the micro-morphology in Zone 2, which presents as reddish brown and gelatinous in Figure 2b. It can be observed that a relatively compact outer rust layer with cracks forms right beneath the ascidians. The outer rust layer is mainly composed of spherical-shaped (Figure 5b) and flowery-shaped (Figure 5c) corrosion products. The spherical-shaped rust mainly appears in the center of the outer rust layer, and the flowery-shaped rust appears at the cracks and the boundary of the outer rust layer. It can be seen from the EDS results that the ratio of Fe and O are all close to 0.5 in both Local Areas 1 and 2, indicating the formation of FeOOH. According to reference [16], it can be deduced that the spherical rust is α-FeOOH and the flower-shaped rust is γ-FeOOH. The presence of the Cl element in the flower-shaped rust suggests the potential existence of β-FeOOH in Local Area 2 [17,18]. Figure 5d shows the micro-morphology of the inner rust layer in the spalling zone of the outer rust layer. A lumpy rust layer can be found in Local Area 3, which is possibly induced by the compressive strains in the rust layer [19]. Moreover, doughnut-shaped rust can also be observed in the spalling zone. Based on the Fe and O ratio (0.61), it can be deduced that the inner layer might be composed of FeOOH and Fe_3O_4.

Figure 6a shows the micro-morphology of the compact black rust layer in Zone 3 beneath the mussels. It can be seen that the rust layer presents as a compact plate shape, with some local damage areas (Figure 6b). Some lamellar structures can be found on the compact plate layer. Loose and porous rust layers can be found beneath the outer compact layer in the local damaged areas (Figures 5d and 6c). The EDS results show that the ratio of Fe and O are all close to 0.5 for the rust layers presented in Figures 5d and 6a, indicating that FeOOH is the main corrosion product beneath the mussels. The globular and bird nest shapes of the rust layer shown in Figures 5d and 6c resemble the typical morphology of γ-FeOOH, as described in reference [14].

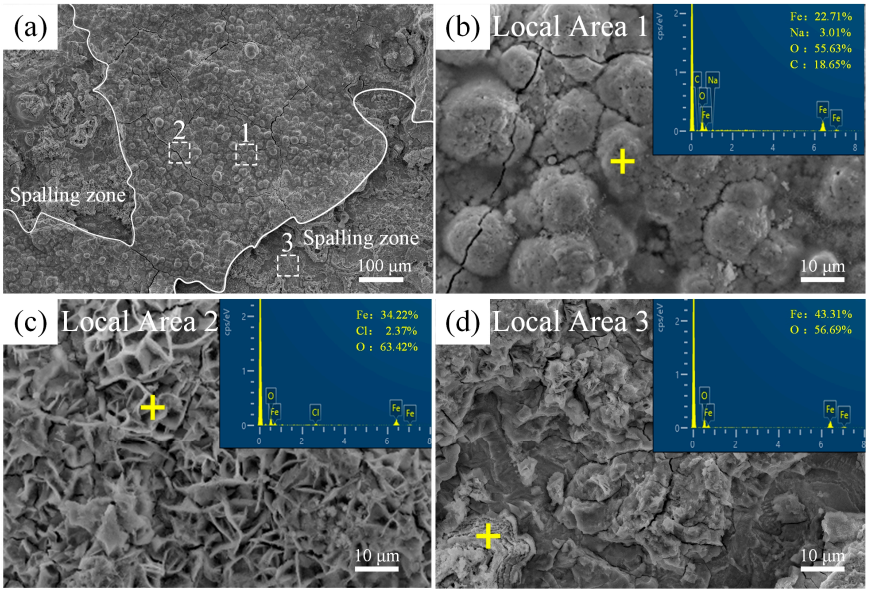


Figure 5. The micro-morphologies of the rusts formed beneath the ascidians: (**a**) the general view of the rust layer in different local areas. The enlargement of the local areas in Figure 5a: (**b**) Local Area 1, (**c**) Local Area 2, and (**d**) Local Area 3.

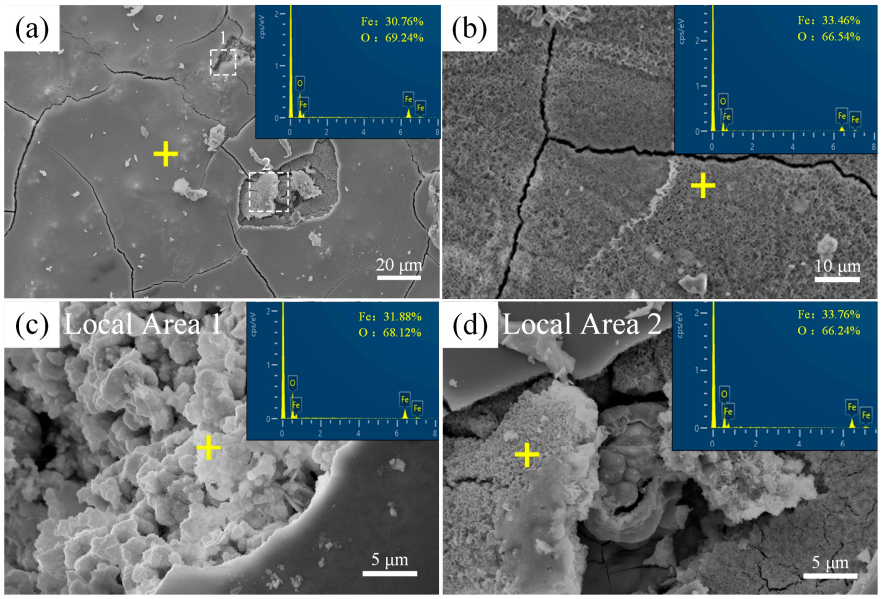


Figure 6. The general micro-morphologies of the rust layers formed beneath the mussels (**a**,**b**) and the enlargement of the local areas in Figure 6a: (**c**) Local Area 1, (**d**) Local Area 2.

It can clearly be seen from the micro-morphology measurement results of the three typical areas that the structure of the rust layer is complex, and it presents as a hierarchical structure. In order to further understand the corrosion process beneath the different marine organisms, cross-section characterizations in combination with local Raman spectroscopy measurements were performed, and the test results of these three typical areas are presented in Figure 7. Raman spectroscopy analysis of the iron oxidations is based on Table 2, which is provided in a previous study [5].

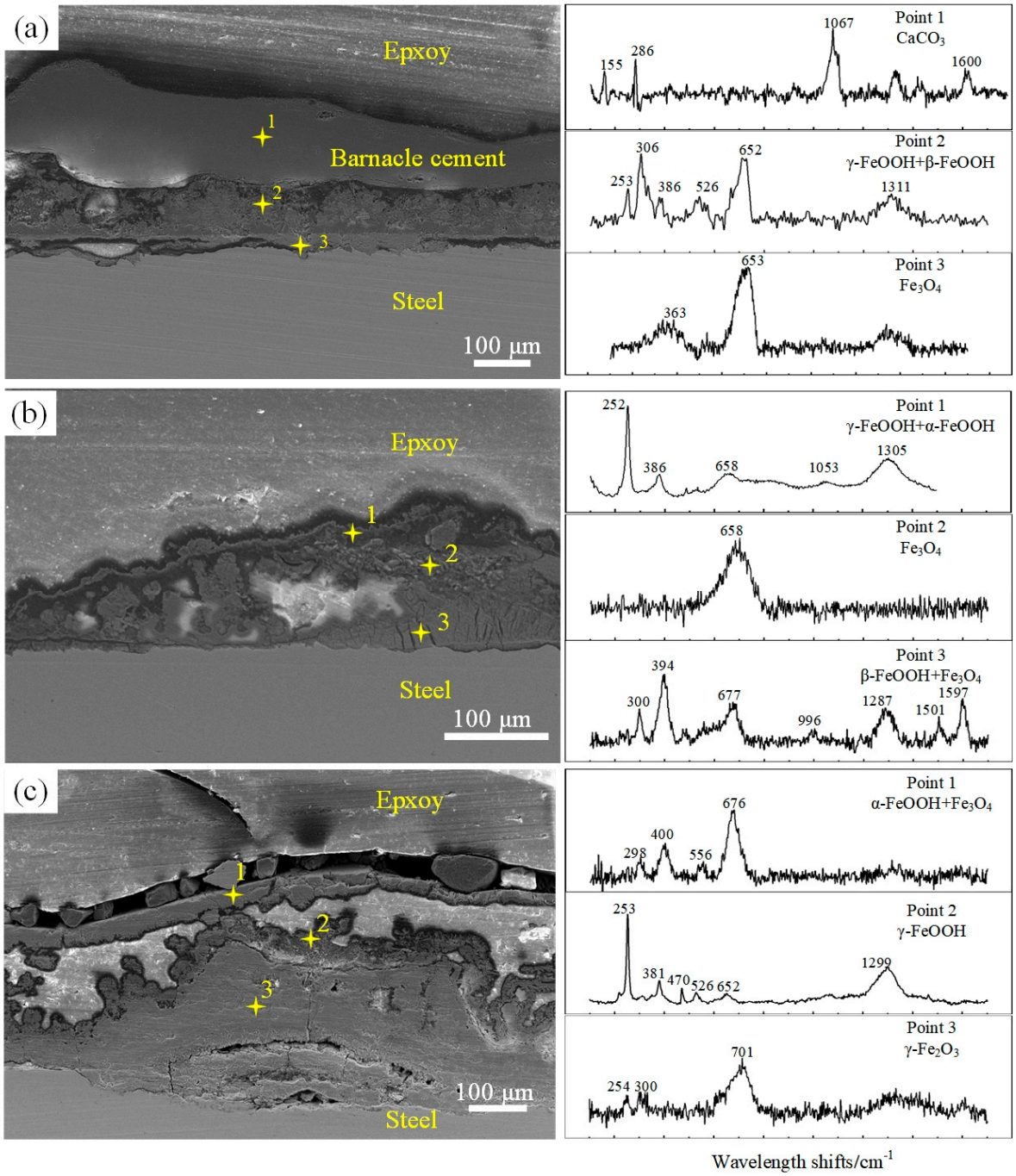


Figure 7. Cross-section views and local Raman spectra measurement results of Areas 1–3 beneath different fouling organisms: (**a**) barnacles, (**b**) ascidians, and (**c**) mussels.

Figure 7a shows a cross-section and the Raman spectra of the rust layer beneath the barnacles. It can be seen that three different layers are observable from a cross-section view. Based on the Raman spectrum measurement, it can be found that the outer layer is $CaCO_3$, with characteristic peaks at 155 cm^{-1}, 286 cm^{-1}, and 1067 cm^{-1} [20]. It can be seen that the barnacles have a great shielding effect through the formation of a compact and thick $CaCO_3$ layer. The interlayer presents as β-FeOOH (characteristic peaks at 306 cm^{-1} and 386 cm^{-1}) and γ-FeOOH (characteristic peaks at 253 cm^{-1}, 526 cm^{-1}, and 1311 cm^{-1}) [14,21]. The inner layer shows that the main corrosion product is Fe_3O_4, with characteristic peaks at 653 cm^{-1} [5].

Figure 7b shows the cross-section and the Raman spectra o the rust layer beneath the ascidians. It can be seen that both the outer and inner rust layers are loose with holes and cracks. The epoxy could flow into the rust layer due to its porous structure. Based on the Raman spectrum measurements, it can be seen that the outer layer is mainly composed of α-FeOOH (characteristic peaks at 386 cm^{-1} and 1053 cm^{-1}) and γ-FeOOH (characteristic peak at 252 cm^{-1} and 1305 cm^{-1}) [22]. The main components of the interlayer are Fe_3O_4, with characteristic peaks at 658 cm^{-1}. The inner layer is mainly composed of β-FeOOH (characteristic peaks at 300 cm^{-1} and 394 cm^{-1}) and Fe_3O_4 (characteristic peaks at 677 cm^{-1}) [14].

Figure 7c shows the cross-section and Raman spectra of the rust layer beneath the mussels. It can be seen that an obvious epoxy layer forms between the outer rust layer and the intermediate rust layer, indicating the local damage of the outer rust layer, which could allow the permeation of the epoxy. This finding corresponds well with that shown in Figure 6, in which cracks and local peeling can be observed. Long cracks can be found in the inner rust layer, indicating that seawater could further penetrate the inner layer. The thickness of the rust layer reaches 402 μm, which is much higher than those formed beneath barnacles (124 μm) and ascidians (96 μm). Based on the Raman spectrum measurement, it can be seen that the outer layer is mainly composed of Fe_3O_4 (characteristic peaks at 556 cm^{-1} and 676 cm^{-1}) and α-FeOOH (characteristic peaks at 298 cm^{-1} and 400 cm^{-1}) [22]. The main component of the interlayer is γ-FeOOH, with characteristic peaks at 253 cm^{-1} and 381 cm^{-1} and 526 cm^{-1} and 1299 cm^{-1} [22]. The inner layer shows the presence of γ-Fe_2O_3, with characteristic peaks at 701 cm^{-1} [5]. It is known that Fe_3O_4 is readily transformed into γ- Fe_2O_3 via laser heating during Raman characterizations [5]. Accordingly, the γ- Fe_2O_3 characteristic peak at 701 cm^{-1} should be regarded as Fe_3O_4.

Table 2. Characteristic wavelength shifts (cm^{-1}) in the main Raman peaks corresponding to rust phases from different bibliographic sources.

Compound	Ref.	Wavelength Shifts (cm^{-1})
γ-FeOOH	[15,16,21]	(248–252) ^{S}, (378–380), (528–530), (1300–1310)
α-FeOOH	[5,19]	(298–301), (385–390) ^{S}, (1000–1120) ^{M}
β-FeOOH	[14,22]	(310–314) ^{S}, (385–390) ^{S}
Fe_3O_4	[5,15]	(540–550), (636–670) ^{S}
γ-Fe_2O_3	[5]	350, (700–720) ^{S}
α-Fe_2O_3	[5]	(220–228) ^{S}, (289–299) ^{S}, (1320–1330) ^{M}

Underlined: the next strongest peak; ^{M}: the magnon peak; ^{S}: the strongest peak.

3.4. The Corrosion Morphologies of the Steel Beneath Different Organisms

The 3D profiles of Areas 1–3 after the removal of the rust layer are depicted in Figure 8. It can be seen from Figure 8a that nearly no corrosion occurs in the central area of the barnacle-covered area. Serious corrosion occurs at the edge of the barnacle, where the corrosion depth reaches 72.6 μm. The serious corrosion at the edge of the barnacle is possibly induced by the crevice between the steel substrate and the hard shell. It can be seen from Figure 8b that general corrosion occurs in the local areas covered by ascidians, where the height fluctuation is less than 19 μm. As shown in Figure 8c, pitting corrosion can be found in the local areas covered by mussels. The pits are dense and small, of which the maximum depth reaches 45.3 μm.

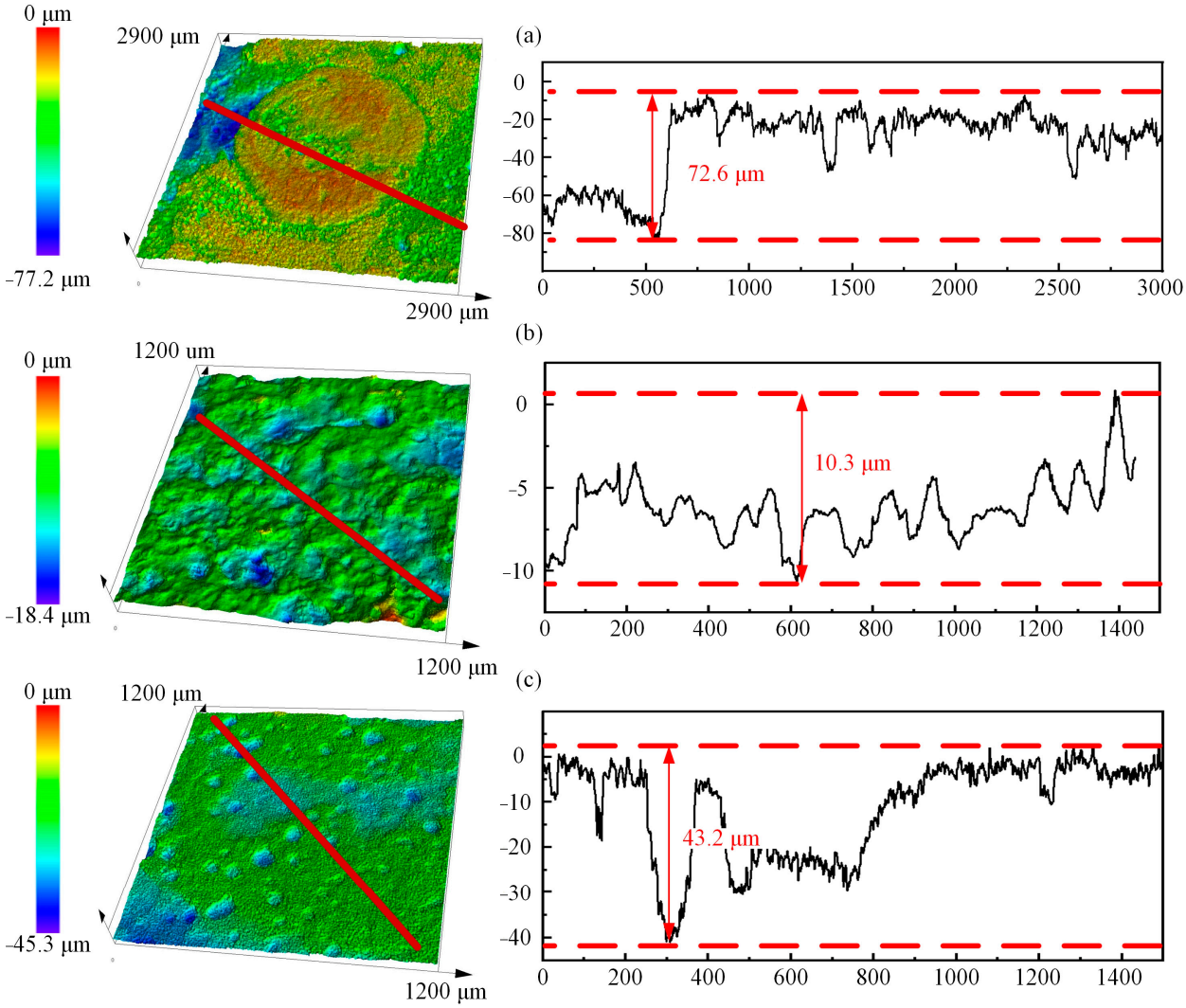


Figure 8. The 3D profiles of Areas 1–3 beneath different fouling organisms: (**a**) barnacles, (**b**) ascidians, and (**c**) mussels.

It can clearly be seen that the different fouling organisms cause totally different corrosion morphologies. Barnacles and mussels, belonging to hard-fouling organisms, cause localized corrosion of carbon steel. On the contrary, ascidians, belonging to soft-fouling organisms, cause general corrosion.

4. Discussion

It can be seen from the test results that the species of fouling organism has a significant influence on the corrosion propagation of carbon steel in the Dalian Sea area. Corrosion initiation and propagation in the Dalian Sea area should be further discussed.

At the initial immersion stage, in January, the temperature of the seawater is around 0 °C, during which no seaweed or marine organisms were found on the steel plate. The corrosion process was totally induced by natural seawater. During this period, an anodic reaction caused the dissolution of the steel substrate.

$$Fe \rightarrow Fe^{2+} + 2e^{-} \quad (1)$$

This is because seawater is weakly alkaline and dissolved oxygen is reduced as an electron acceptor to equilibrate the anode reaction [23]. Thus, the cathodic reaction is the oxygen reduction at the beginning of the test.

$$O_2 + 2H_2O + 4e^- \rightarrow 4OH^- \quad (2)$$

$$Fe^{2+} + 2OH^- \rightarrow Fe(OH)_2 \quad (3)$$

With immersion time lengthening, the hydroxides dehydrate and convert into stable oxides due to the oxidation of dissolved oxygen and the catalytic action of chloride ions [12]. The following shows a series of reactions:

$$Fe(OH)_2 + Cl^- \rightarrow Fe(OH)^+ + OH^- + Cl^- \quad (4)$$

$$\begin{gathered} 4Fe(OH)^+ + 4OH^- + O_2 \rightarrow 4\beta - FeOOH + 2H_2O \\ \text{or} \\ 4Fe(OH)^+ + 4OH^- + O_2 \rightarrow 4\gamma - FeOOH + 2H_2O \end{gathered} \quad (5)$$

Seaweed began to grow on the steel plate in March when the water temperature gradually increased to above 5 °C, providing a warm bed for the growth of larvae. Obvious larva was found in May, which grew rapidly during this time. Different types of macrofouling organisms could be clearly observed at the beginning of July. In this case, different corrosion behaviors would occur due to the growth of the different marine organisms. A model of the corrosion mechanism of steel with the adhesion of different marine organisms is depicted in Figure 8.

For the barnacle/steel interface, the barnacles adhered to an already-formed rust layer by secreting cement. As shown in Figure 7a, the barnacle cement was compact and flat, which has a strong shielding effect for ions and oxygen diffusion [5]. It can be seen that the rust layer beneath the barnacle cement is composed of γ-FeOOH and β-FeOOH, which are unstable phases. γ-FeOOH and β-FeOOH prefer to change into more stable α-FeOOH or Fe_3O_4 phase after long-term immersion in seawater [22]. Accordingly, the remaining γ-FeOOH and β-FeOOH in the interlayer indicate that the covering of the dense barnacle cement could retard the corrosion process. Serious corrosion would occur at the edge of the barnacles due to the oxygen concentration cell, which was also reported in previous studies [5]. As shown in Figure 9a, the formation of Fe_3O_4 in the center of the barnacle suggests that the central area covered by barnacles is a cathodic region, along with the occurrence of a cathodic reaction [24].

$$8\beta - FeOOH/\gamma - FeOOH + Fe^{2+} + 2e^- \rightarrow 3Fe_3O_4 + 4H_2O \quad (6)$$

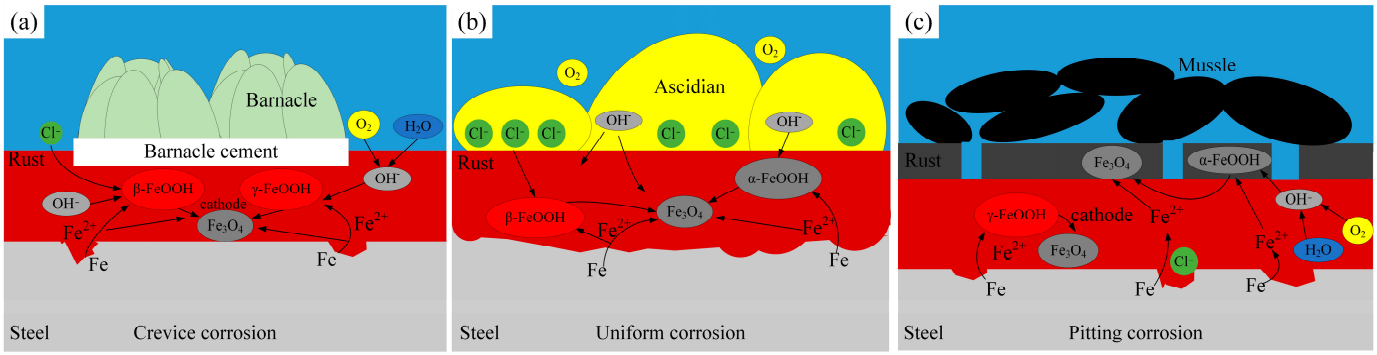


Figure 9. Model of the corrosion mechanism of the carbon steel with (**a**) barnacle adhesion, (**b**) ascidian adhesion, (**c**) mussel adhesion.

For the ascidian/steel interface, uniform corrosion was found with a relatively low surface height fluctuation. It can be reported that ascidians have a tiny influence on the local chemical environment because the bodies of ascidians are wrapped in a capsule of colloids or similar plant cellulose, which has excellent conductivity and ion diffusivity [6]. Therefore, the interface of ascidian barnacles exhibits uniform electrochemical characteristics. In addition, according to the cross-section views in Figure 8b, the presence of hole and

epoxide infiltration areas in the rust layer beneath the ascidians can be observed. This indicates that the rust layer was sufficiently loose to allow the penetration of seawater into the steel substrate, causing general corrosion under the ascidians. Moreover, as shown in Figure 8b, ascidian secretions can cause local accumulation of chloride ions [6], resulting in the formation of β-FeOOH at the inner layer. Meanwhile, the covering by sea squirts isolates oxygen and changes the cathode reaction from oxygen reduction to the reduction of hydroxyl iron oxide (Reaction 6).

For the mussel/steel interface, pitting corrosion was the main corrosion pattern (Figure 8c). Although barnacles and mussels are both hard-fouling organisms, the adsorption capacity of mussels is much lower than that of barnacles. The adhesion of mussels to the rust layer is point adhesion, as mussels normally adhere to steel through filamentous secretions [13]. Accordingly, the shielding effect induced by mussels is much lower than by barnacles. The formation of stable Fe_3O_4 and α-FeOOH beneath the mussels further verifies the weak adhesion effect. The local damage points of the rust layer would allow the penetration of seawater in local areas. Due to the inhomogeneous distribution of the seawater beneath the rust layer, pitting corrosion would occur in the local damaged areas due to the introduction of more chloride ions. The relatively compact outer rust layer could provide an occlusive area for pitting propagation.

5. Conclusions

Based on the test results, it can be concluded that barnacles, ascidians, and mussels are the main macro-fouling organisms that cause corrosion on carbon steel in the Dalian Sea area. Each of these organisms leads to different corrosion patterns. The covering of barnacles hinders corrosion in the central area of the steel, but it can lead to severe crevice corrosion at the edge of the tough shell. The adhesion of ascidians, on the other hand, has minimal impact on the corrosion process due to their excellent conductivity and ion diffusivity. General corrosion occurs beneath ascidians. Pitting corrosion can be observed on carbon steel covered by mussels. Seawater easily seeps into mussels and the damaged outer rust layer, creating a localized occlusive area that promotes pitting propagation.

Author Contributions: Conceptualization, W.C. and Y.X.; methodology, W.C., Y.W., M.W., Y.H. and Y.X.; supervision and funding acquisition, Y.H. and Y.X.; writing—original draft, W.C. and Y.W.; writing—review and editing, Y.X. and W.C. All authors have read and agreed to the published version of the manuscript.

Funding: This research was funded by the National Key Research and Development Program (No.: 2022YFC2806204) and the Natural Science Foundation of China (No.: 52001055).

Data Availability Statement: Not applicable.

Acknowledgments: The authors acknowledge the financial support from the National Key Research and Development Program: 2022YFC2806204; the Natural Science Foundation of China: 52001055.

Conflicts of Interest: The authors declare no conflict of interest.

References

1. Dang, H.; Liang, A.; Feng, R.; Zhang, J.; Shao, Y.; Yam, M.C.H. Experiments on static and fatigue behavior of corroded Q235B and 42CrMo steels. *J. Constr. Steel Res.* **2022**, *198*, 107535. [CrossRef]
2. Xu, Y.; Zhang, Q.; Chen, H.; Huang, Y. Understanding the interaction between erosion and corrosion of pipeline steel in acid solution of different pH. *J. Mater. Res. Technol.* **2023**, *25*, 6550–6566. [CrossRef]
3. Jiang, W.H.; Zhang, Q.L.; Niu, L.; Liu, L.; Huang, Y. Corrosion Behavior of 921A High Strength Carbon Steel in Flowing Natural Seawater. *Mater. Rep.* **2023**, *37*, 22030153.
4. Wang, Z.; Huang, Y.; Wang, X.; Xu, Y.; Cai, F. Effects of oyster as macrofouling organism on corrosion mechanisms of a high-strength low-alloy steel. *Corros. Sci.* **2022**, *207*, 110580. [CrossRef]
5. Cai, F.; Huang, Y.; Xing, S.; Xu, Y.; Zhao, X.; Wang, X.; Wang, Z.; Ringsberg, J.W. Characteristics and mechanisms of low-alloy high-strength steel corrosion behavior under barnacle adhesion based on a comparison experiment. *Corros. Sci.* **2023**, *217*, 111146. [CrossRef]

6. Wang, Z.; Wang, X.; Huang, Y.; Zhou, H.; Wu, Y.; Sun, Y.; Nan, Y.; Xu, H.; Pu, J.; Hou, B. Macrofouling organisms: Protection or damage of steel in marine environments? *Corros. Sci.* **2023**, *212*, 110928. [CrossRef]
7. Blackwood, D.J.; Lim, C.S.; Teo, S.L.M.; Hu, X.; Pang, J. Macrofouling Induced Localized Corrosion of Stainless Steel in Singapore Seawater. *Corros. Sci.* **2017**, *129*, 152–160. [CrossRef]
8. Zhang, Z.; Li, Z.; Wu, F.; Xia, J.; Huang, K.; Zhang, B.; Wu, J. A comparison study of crevice corrosion on typical stainless steels under biofouling and artificial configurations. *npj Mater. Degrad.* **2022**, *6*, 85. [CrossRef]
9. Chen, W.; Wang, M.; Li, M.; Li, K.; Huang, Y.; Xu, Y. Interaction of marine organisms on localized corrosion of 316L stainless steel in Dalian seawater. *Anti-Corros. Methods Mater.* **2023**, *70*, 157–165. [CrossRef]
10. Ma, S.; Sun, H.; Huang, G.; Zhu, X. Effect of Marine fouling Creatures on Corrosion of Carbon Steel. *J. Chin. Soc. Corros. Prot.* **2000**, *20*, 177–182.
11. Sun, H.; Wang, Z.; Gao, P.; Liu, P. Selection of aquatic plants for phytoremediation of heavy metal in electroplate wastewater. *Acta Physiol. Plant.* **2013**, *35*, 355–364. [CrossRef]
12. Yang, J.; Lu, Y.; Guo, Z.; Gu, J.; Gu, C. Corrosion behaviour of a quenched and partitioned medium carbon steel in 3.5wt.% NaCl solution. *Corros. Sci.* **2018**, *130*, 64–75. [CrossRef]
13. Chang, Z.; Shen, Y.; Xue, J.; Sun, Y.; Zhang, S. Multifunctional soy protein gels with excellent initial adhesion and bonding strength based on a mussel-inspired redox self-catalytic and oyster-inspired organic-inorganic hybrid dual-bionic strategy. *Ind. Crops Prod.* **2023**, *195*, 116430. [CrossRef]
14. Alcántara, J.; Chico, B.; Díaz, I.; de la Fuente, D.; Morcillo, M. Airborne chloride deposit and its effect on marine atmospheric corrosion of mild steel. *Corros. Sci.* **2015**, *97*, 74–88. [CrossRef]
15. Alcántara, J.; Chico, B.; Simancas, J.; Díaz, I.; de la Fuente, D.; Morcillo, M. An attempt to classify the morphologies presented by different rust phases formed during the exposure of carbon steel to marine atmospheres. *Mater. Charact.* **2016**, *118*, 65–78. [CrossRef]
16. Morcillo, M.; Chico, B.; Alcantara, J.; Díaz, I.; Wolthuis, R.; Fuente, D. SEM/Micro-Raman Characterization of the Morphologies of Marine Atmospheric Corrosion Products Formed on Mild Steel. *J. Electrochem. Soc.* **2016**, *163*, C426–C439. [CrossRef]
17. Song, X.; Boily, J. Variable Hydrogen Bond Strength in Akaganéite. *J. Phys. Chem. C* **2012**, *116*, 2303–2312. [CrossRef]
18. Xiao, H.; Ye, W.; Song, X.; Ma, Y.; Li, Y. Formation process of akaganeite in the simulated wet-dry cycles atmospheric environment. *J. Mater. Sci. Technol.* **2018**, *34*, 1387–1396. [CrossRef]
19. Zhang, H.; Xu, J.; Guo, L.; Dong, H. Study on rust layers of carbon steel, weathering steel and alloy steel exposed to Shanghai atmosphere for three years. *Mater. Today Commun.* **2023**, *35*, 105520. [CrossRef]
20. Badou, A.; Pont, S.; Auzoux-Bordenave, S.; Lebreton, M.; Bardeau, J. New insight on spatial localization and microstructures of calcite-aragonite interfaces in adult shell of *Haliotis tuberculata*: Investigations of wild and farmed abalones by FTIR and Raman mapping. *J. Struct. Biol.* **2022**, *214*, 107854. [CrossRef]
21. Fan, Y.M.; Liu, W.; Sun, Z.T.; Chowwanonthapunya, T.; Zhao, Y.G.; Dong, B.J.; Zhang, T.Y.; Banthukul, W. Effect of chloride ion on corrosion resistance of Ni-advanced weathering steel in simulated tropical marine atmosphere. *Constr. Build. Mater.* **2021**, *266*, 120937. [CrossRef]
22. de la Fuente, D.; Alcántara, J.; Chico, B.; Díaz, I.; Jiménez, J.A.; Morcillo, M. Characterisation of rust surfaces formed on mild steel exposed to marine atmospheres using XRD and SEM/Micro-Raman techniques. *Corros. Sci.* **2016**, *110*, 253–264. [CrossRef]
23. Gong, K.; Wu, M.; Liu, G. Comparative study on corrosion behaviour of rusted X100 steel in dry/wet cycle and immersion environments. *Constr. Build. Mater.* **2020**, *235*, 117440. [CrossRef]
24. Wang, Y.; Mu, X.; Chen, Z.; Lin, Z.; Dong, J.; Daniel, E.F.; Qi, J.; Ke, W. Understanding the role of alloyed Cu and P in the initial rust composition of weathering steel formed in a simulated coastal-industrial atmosphere. *Corros. Sci.* **2021**, *193*, 109912. [CrossRef]

Disclaimer/Publisher's Note: The statements, opinions and data contained in all publications are solely those of the individual author(s) and contributor(s) and not of MDPI and/or the editor(s). MDPI and/or the editor(s) disclaim responsibility for any injury to people or property resulting from any ideas, methods, instructions or products referred to in the content.